MONITORING AND IDENTIFICATION OF PROGRESSIVE DAMAGE IN FIBER REINFORCED COMPOSITE STRUCTURES USING NON-DESTRUCTIVE TESTING

By Utku Guclu

Submitted to
the Graduate School of Engineering and Natural Sciences
in partial fulfillment of
the requirements for the degree of
Master of Science

SABANCI UNIVERSITY

December 2018

MONITORING AND IDENTIFICATION OF PROGRESSIVE DAMAGE IN FIBER REINFORCED COMPOSITE STRUCTURES USING NON-DESTRUCTIVE TESTING

APPROVED BY:

Prof. Dr. Mehmet Yıldız
(Thesis Supervisor)

Assoc. Prof. Dr. Burç Mısırlıoğlu

Asst. Prof. Dr. Bertan Beylergil

DATE OF APPROVAL: 27.12.2018

Monitoring and Identification of Progressive Damage in Fiber Reinforced Composite Structures using Non-Destructive Testing

Utku Guclu

MAT, M.Sc. Thesis, 2019

Thesis Supervisor: Prof. Dr. Mehmet Yıldız

Abstract

This study focuses on the connection between damage progression and non-destructive testing techniques to evaluate the feasibility of these techniques for structural health monitoring. For this aim, three different techniques, acoustic emission (AE), digital image correlation (DIC) and infrared thermography (IRT), were selected deliberately due to their focus on detecting the three different manifestations of energy that originates from damage. Feasibility of these techniques were assessed on carbon fiber reinforced composites with two different stacking sequences under static loading conditions. Static loading conditions were selected to have less noise in the AE and the IRT data. Moreover, two different stacking sequences provided a better understanding on the response of non-destructive testing techniques.

Fiber Takviyeli Kompozit Yapılarda İlerleyen Hasarin Denetlenmesi ve Tanımlanması

Utku Guclu

MAT, M.Sc. Thesis, 2019

Tez Danışmanı: Prof. Dr. Mehmet Yıldız

Anahtar Kelimeler: *yapısal sağlık gözetimi (SHM),* tahribatsız muayine teknikleri *(NDT),* akustik emisyon (AE), dijital görüntü korelasyonu (DIC) ve kızılötesi termografi (IRT)

Abstract

Bu çalışma, yapısal sağlığın izlemesi için tahribatsız muayine tekniklerinin uygulanabilirliğini ve hasarın ilerlemesi arasındaki bağlantıya odaklanmaktadır. Bu amaç için, üç farklı teknik, akustik emisyon (AE), dijital görüntü korelasyonu (DIC) ve kızılötesi termografi (IRT) seçildi. Bu teknikler hasardan kaynaklanan üç farklı enerji tezahürünü tespit etmeye odaklandıklarından kasten seçildi. Bu tekniklerin uygulanabilirliği, statik yükleme koşulları altında iki farklı istifleme sekansı olan karbon fiber takviyeli kompozitler üzerinde değerlendirildi. Statik yükleme koşulları AE ve IRT verilerinin daha az gürültüye sahip olması için seçilmiştir. Ayrıca, iki farklı istifleme dizisi, tahribatsız test tekniklerinin tepkisi hakkında daha iyi bir anlamak için seçilmiştir.

ACKNOWLEDGEMENT

I would like to thank to;

Professor Mehmet Yıldız for patiently guiding not just this thesis work and my engineering career as well.

Jury members, Assoc. Prof. Dr. Burç Mısırlıoğlu and Asst. Prof. Dr. Bertan Beylergil for their time and highly valuable critics to make this thesis worth reading.

Folks at Integrated Manufacturing Technologies Research and Application Center, Çağatay Yılmaz, Çağdaş Akalın, Jamal Zanjani and Isa Tabrizi for having meaning more than teammates.

Table of Contents

List of Figures

CHAPTER 1

1   Introduction

1.1   Motivation

Composite structures are used in a wide range of applications such as in aerospace and other branches of the transportation industry. For example, the Boeing 787-8 consists of 50 percent composite structures by weight (Figure 1.1). High specific strength/stiffness of these materials is the main driving force behind the increasing trend of using composite structures. Composite materials also contribute to the reduction of the weight of the vehicle, to greater efficiency in the consumption of fuel due to their high specific strength/stiffness. This can be achieved by precisely selecting the composite material for the specific application that it is designed for. Therefore, the rise of composite structures enable a material to be designed for its specific structural conditions whereas before design could only improve as far as material would allow.
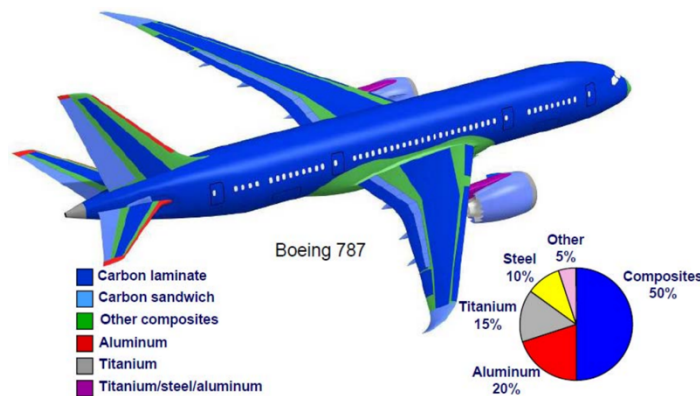
Figure 1.1- Bill of Materials for Airbus 380 [1]

Moreover, composite structures have better corrosion resistance and longer fatigue life compared to conventional materials such as aluminum and steel. The high percentage of polymer in a composite structure results in good corrosion whereas its heterogeneous structure increases the fatigue life because if a ply is damaged or failed, other plies can still bear the load. Unlike conventional metals, since there is no continuous structure, a crack cannot propagate through multiple plies. Therefore, each individual ply fails at different stages of the lifetime.

In conventional metals, damage mainly occurs due to fatigue loading and it is easy to detect fatigue and/or stress corrosion cracks before catastrophic failure in most cases. However, in composite structures, existence of damage is independent of existence of visible or surface based damage. Therefore, it is time consuming to inspect the progression of damage in composite structures and very difficult to detect the formation of damage. Motivation behind this thesis is to monitor and identify damage within composite structure by using common non-destructive testing techniques. For this aim, three non-destructive testing techniques, acoustic emission (AE), digital image correlation (DIC) and infrared thermography (IRT), are selected that are complementary to each other in terms of energy. The complementary nature is of these techniques is due to they all measuring different manifestations of the same energy that originates due to damage. AE is used to investigate the elastic waves, DIC investigates the strain and IRT investigates the absorption and release of thermal energy due to loading and structural deformation.

1.2   Outline of the Thesis

Chapter 2 of this thesis covers the literature review on failure mechanisms of composite structures, capabilities of non-destructive techniques and hot press manufacturing technique. Chapter 3 covers the experimental set up of the each non-destructive testing technique and the manufacturing conditions for samples. Chapter 4 covers experimental results and discussion for each testing technique individually, then couples these results to discuss damage progression with the specimen. Chapter 5 concludes this thesis.

CHAPTER 2

Literature Review

2.1   Fiber reinforced Composite Structures

Composite structures are made up of two or more structural elements. First of these elements is a fiber which is the load bearing element and the other is a polymer which is the reinforcing element. Depending on the application, the fiber element can be carbon, glass, kevlar or boron. Each of these fiber types have a different tensile strength and stiffness. They are selected according to these parameters.

2.2   Failure Mechanisms of Fiber Reinforced Composite Structures

Failure mechanisms of failure mechanisms of fiber reinforced composite structures depend on various aspects such as fiber and matrix properties, volume fraction of fibers and matrix, ply orientation and stacking sequence. Failure arises as a result of multiple failure mechanisms. These mechanisms are matrix cracking, delamination, fiber matrix debonding, fiber failure and fiber pull-out (Figure 2.1).

For non-destructive evaluation purposes these mechanisms are characterized in terms of their formation energy and formation duration. Formation energy relates with the stress level that the mechanism fails and the formation duration may relate to the ductility and the brittleness of the failure of the mechanism.
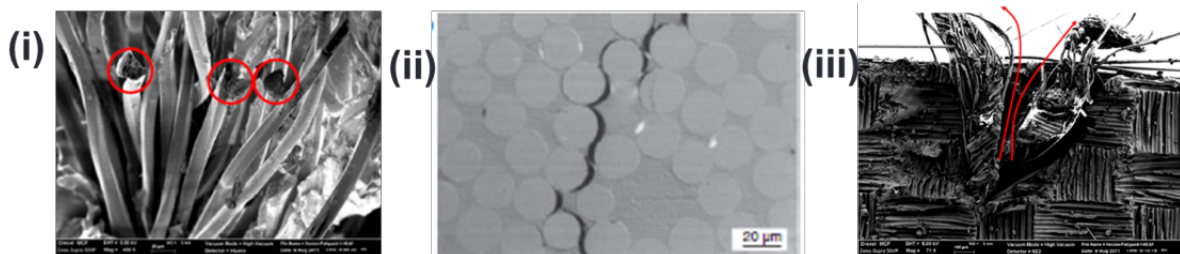
Figure 2.1- Failure mechanisms of FRPC. (i) Fiber failure, (ii)Matrix crack, (iii) Delamination [2]

2.3   Non Destructive Testing

There are type two types of non-destructive testing which are active and passive techniques. In order to inspect damage on or within a material, active techniques have built in sources that can generate a pulse, a wave, a magnetic field, etc. In industry, active techniques are usually used to monitor the location and the size of damage.

Passive techniques require a change in the material to gather information. They are most commonly used in research to characterize the behavior of a material subjected to the different types of loading. The information is gathered by passively observing for the initiation and the propagation of damage as it happens. Data from research can be used to create standards for the industry in terms of significance of a defect size or location.

i.   AE

Acoustic emission is a phenomenon that occurs due to a sudden change in a material. A sudden change acts as a source and generates elastic waves that propagate throughout the material (Figure 2.2). Therefore, as material deforms, any source through the volume of the material generate acoustic emissions in terms of elastic waves which can be collected and characterized. It must be noted that every acoustic emission consists of elastic waves which are recorded as waveforms. However, not every elastic wave is an acoustic emission.
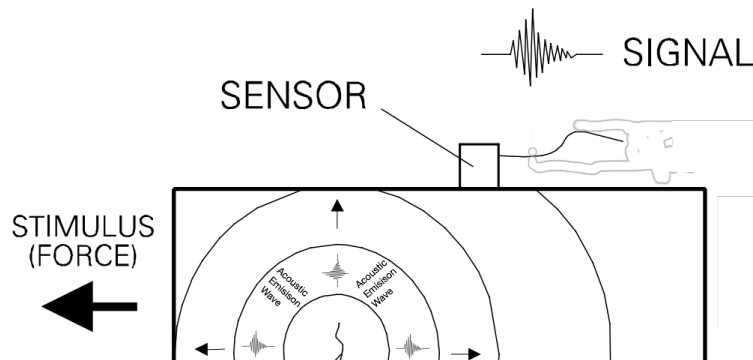
Figure 2.2- Working Principle of AE Testing [3]

These emissions are collected by piezoelectric sensors that are attached to the surface of the specimen. Sensors convert the mechanical vibrations of elastic waves into electrical signals which are characterized by using various signal processing features. These features are split in two groups, first is the waveform based features and next are the wave energy based features. [4]

Waveform based features are dependent on the origination characteristics an acoustic emission source. For example, each frequency based characteristic is a waveform based. This is due to the nature of frequency that is dependent on origination time of an acoustic emission. An acoustic emission that is generated in a short amount of time will have a high oscillation rapidly which in other words is high frequency. Due to source dependency of these features, they are valuable for characterizing acoustic emission sources. More importantly waveform based features are dependent on the material composition therefore, they are a material property which would remain constant for the same composition.
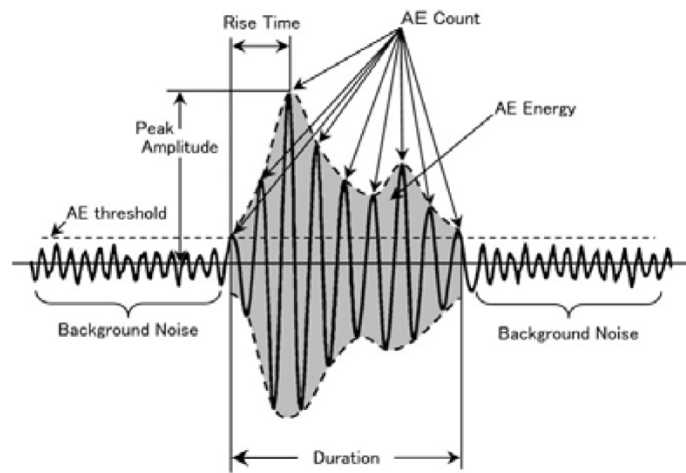
Figure 2.3- Waveform features [5]

On the other hand, energy based features are dependent on the material properties, medium and sensor placement. Similar to waveform based features, origination energy of a wave is based on the composition of the material. However, the originating energy is not the same as recorded energy. As the wave propagate through a medium and collected by the sensor, it is attenuates. Even if the origination energy of similar sources are the same, recorded energy might not be similar. Therefore, energy based features can be misleading and can change depending on the material properties (related with attenuation). Consequently, energy based features can display the relative trend within a sample. However, comparing the magnitude of damage between samples by using energy can be misleading. Energy features that are used in this thesis will be explained in results and discussion section (Figure 4.3).

Lastly there are coupled features that uses both waveform and energy based features. These features are recently becoming popular due to characterizing each waveform in an additional dimension. An example of a coupled feature is the partial power. Each partial power is given a frequency range where the partial power takes the ratio between the complete energy of the waveform and the energy of the defined frequency range. Thus, partial power can negate the effects of attenuation by quantifying the magnitude of each frequency range in relation to each other. Table 1 is an example of partial power integrals where PP1 is between 0 – 200 kHz, PP2 is between 200 – 400 kHz, PP3 is between 400 – 600 kHz, PP4 is between 600 – 800 kHz. [6-10]

Table 1- Partial Power Integrals [6]

Partial Power 1 (PP1)	$\int_{0}^{200\,kHz} \hat{U}^{2}(f)df \, / \int_{0}^{2500} \hat{U}^{2}(f)df$
Partial Power 2 (PP2)	$\int_{200}^{400\,kHz} \hat{U}^{2}(f)df \, / \int_{0}^{2500} \hat{U}^{2}(f)df$
Partial Power 3 (PP3)	$\int_{400}^{600\,kHz} \hat{U}^{2}(f)df \, / \int_{0}^{2500} \hat{U}^{2}(f)df$
Partial Power 4 (PP4)	$\int_{600}^{800\,kHz} \hat{U}^{2}(f)df \, / \int_{0}^{2500} \hat{U}^{2}(f)df$

The motivation behind coupled features such as partial powers is are effective characterizing acoustic emissions with more than one source. Reasoning behind multiple source acoustic emissions can be explained by the way that the waveforms are collected. Waveform of the acoustic emission starts to be collected after a specified amplitude level is passed. This is done to differentiate a waveform from mechanical noise. After acquisition of the waveform begins, it continues until the waveform drops below specified amplitude level or a certain time limit is reached (max duration is 2000 microseconds). If he waveform of the acoustic emission has only one dominant frequency, it is generated by a single source. However, if an emission have multiple sources, waveform has multiple different frequencies. Figure 2.4 displays the difference of these two types of waveforms. The reason for multiple emissions to be in the same waveform is that, damage within the material can occur in a rapid sequence that is almost simultaneous (within 100 microsecond). For example fiber breakage can be followed up with delamination and matrix failure. Therefore, the dominant characteristic of a multiple source waveform should be unwounded. [6-10]
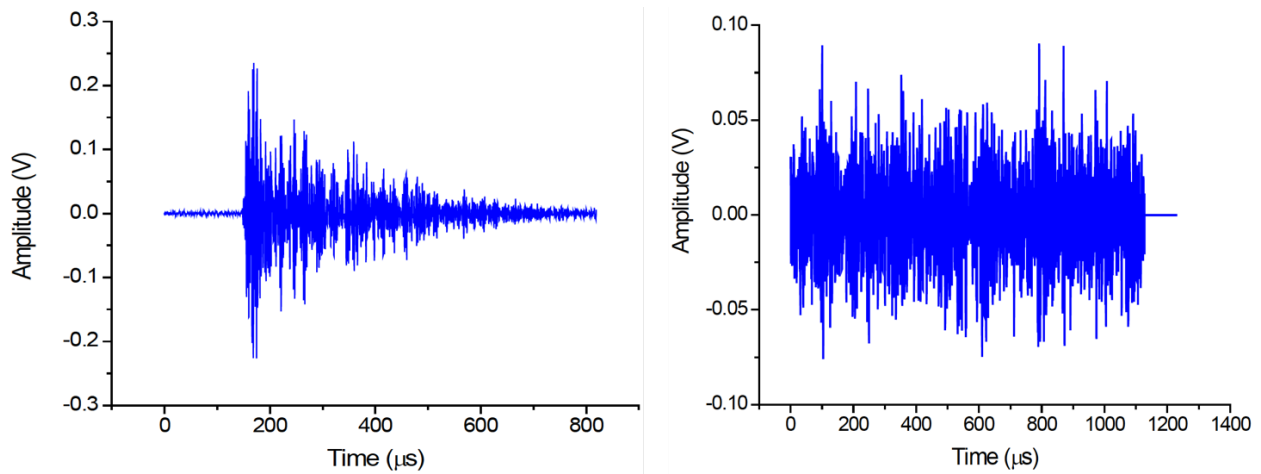
Figure 2.4- Waveform with single dominant frequency (left), Waveform with multiple frequencies (right) [6]

The work of Gutkin et al. [11] stands out as he has characterized failure mechanisms of carbon fiber reinforced polymer composites meticulously. The study was able to induce each failure mechanism and detect the peak frequency resulting from the induced damage. As a result, the study was able to determine frequency ranges for each failure mechanism. Figure 2.5 shows the frequency ranges that Gutkin et al. was able to determine. Even if both this study and Gutkin et al. have similar composite structures, no material can have an exact similar frequency range. However, the frequency distribution (relative differences in frequency) for the failure mechanisms are going to be similar for each carbon fiber based materials. Therefore, Figure 2.5 will be used as a guide to determine the sources of clusters.
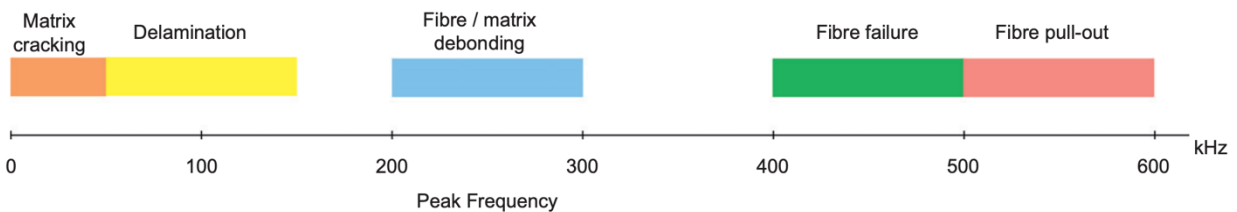
Figure 2.5- Characterization of failure mechanisms in terms of frequency [11]

Clustering is a tool to characterize similar waveforms using additional dimensions. This study follows the work of Kempf et al. [11] as a guide at using K-means clustering. K-means method uses two dimensions to separate the centers of the conglomerated data for clustering.

Parameters selected for K-means clustering for this study is weighted peak frequency and partial power 2. **Error! Reference source not found.** represents weighted peak frequency (f_{WPF}). According to Sause et al. it is the most accurate way to determine the dominant frequency of a waveform. This study was also able to come to the same conclusion on this feature.

$$f_{WPF} = \sqrt{f_{peak} \cdot f_{centroid}} \qquad (1)$$

ii.   Digital Image Correlation

Digital image correlation is a non-contact method that uses data points on a specimen's surface to measure three dimensional displacement and to calculate mechanical deformation features from the measured displacement. Since it is a passive method, loading of the material is required. There has to be a high contrast surface such as a black and white speckle pattern to distinguish these data points (Figure 2.6) on the surface of the specimen. To achieve this pattern, hundreds of black data points are sprayed on to a white background to create a speckle pattern.
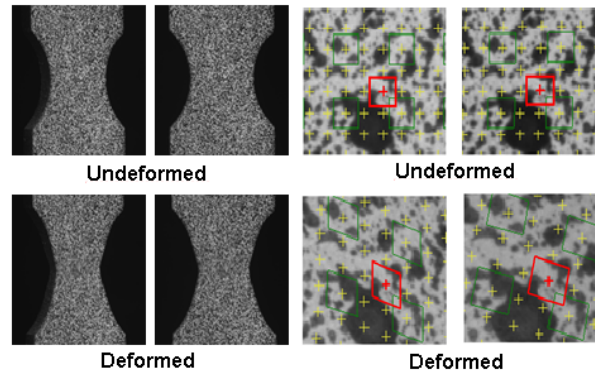
Figure 2.6- Calculation Systematic of DIC

System uses each speckle as a node with a known three dimensional coordinate. Under loading, a sampling frequency is assigned to the system to determine the resolution of the data collected. Dependent on the sampling frequency, system takes multiple images per second to measure the displacement between the data points. Then, the system calculates the localized strain using complex algorithms. This data is used to locate strain concentration points to detect the incipient damage spots. These spots are called hot spots, shown in Figure 2.7 and they indicate the location where the damage is anticipated to occur.
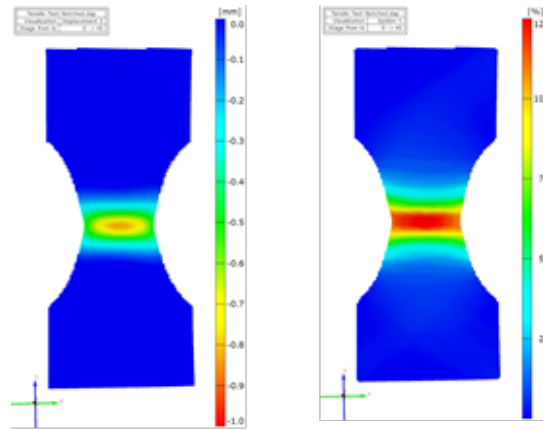
Figure 2.7- An Example of Surface Strain Map

DIC can also be used to calculate any parameter that is the function of strain. After the system calculates strain for each data point, custom functions can be used to transform strain data. Additionally, load data can be uploaded via analog inputs. Therefore, DIC system is able to calculate parameters such as elastic modulus, poisons ratio etc. in all three dimensions. Moreover, these calculated parameters can also be visualized in full field map such as in Figure 2.7.

iii.   Infrared Thermography

Infrared thermography has various applications such as active thermography, lock-in thermography, pulse thermography etc. In this thesis, passive thermography was used to monitor the change in temperature of the sample and detect damage. For this aim, an infrared camera was used to measure the temperature of the sample while it is being loaded. The most important point in the application of passive thermography is to shield the sample from any heat sources. The motivation is to create an adiabatic testing condition and to reduce noise.

IRT uses an infrared sensor to capture the heat radiation that is being emitted by the sample. Similar to a normal camera converting visual spectrum radiation into voltage, infrared sensor converts infrared radiation into voltage. As a result, a field map of the temperature can be obtained where each pixel of the infrared sensor provides temporal information. Change in temperature in static loading have two different sources. These are the elastic deformation and the plastic deformation. During elastic deformation, volume increases and consequently internal energy decreases. Under uniaxial static loading, the relationship between stress and temperature is given

by the Equation (1). This equation states that, as the stress on the sample increases, the temperature will decrease in the case of elastic deformation.

$$\Delta T = - \frac{\alpha}{\rho C_p} T_0 \Delta \, (\sigma_x + \sigma_y + \sigma_z)$$

(2)

Relationship between stress and temperature is much more complicated during plastic deformation where each damage acts as a heat source within the material and increases its temperature. Moreover, in the plastic region elastic deformation continues to occur. Therefore, even though there is a trend of increasing temperature due to damage, sample will continue to cool down if no damage occurs for a span of time.

Risitano et al. [15] studied the temperature response of carbon fiber reinforced polymers under uni-axial static conditions. This study focused on the difference in change in temperature between theoretical and experimental results under static loading. Figure 2.8 shows the theoretical and experimental results obtained by Risitano et al. [15]. Theoretical results is a combination of multiple different equations where the elastic region is linear and the plastic region exponential. Experimental results behave as expected by decreasing in elastic region then increasing in plastic region. Theoretical and experimental results do not match very well but the point of transition was correctly determined. Risitano et al. [15] denoted this transition point from elastic deformation to plastic deformation as the damage stress point where irreversible structurally significant damage starts occurring within the sample. Conclusively even though the transition of elastic and plastic deformation are not visible in stress/strain spectrum, it is possible to distinguish it with thermography.
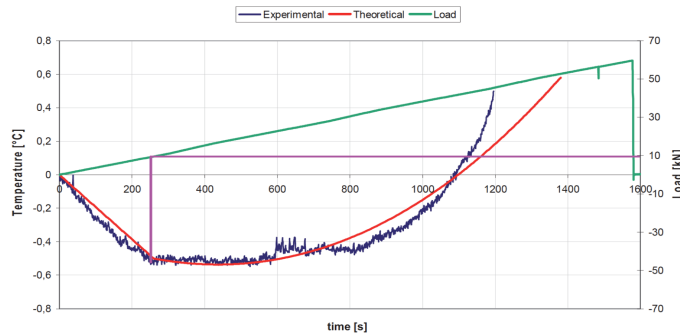
Figure 2.8- Risitano et al. experimental and theoretical results [15]

10

CHAPTER 3

<p style="text-align:center">3   **Experimental Setup**</p>

3.1   Testing Equipment Setup

      i.   Hybrid Testing Setup

The hybrid testing setup (Figure 3.1) is the combination of DIC system, AE system, IRT system and the Instron servo-hydraulic machine (with a 100 kN load capacity) under 1mm/min displacement rate. This setup provides the ability to collect every signature during deformation. Stress concentrations at specific points initiate cracks or grow a deformation, this stress is dissipated by creating new surface. This action produces elastic waves and energy release that can be picked up by non-destructive testing sensors. The elastic waves are collected by AE testing, the strain that is created by the creation of a new surface is collected by DIC and temperature change due to thermoelastic effect and damage is collected by IRT. Data collected using these techniques are correlated with the data from the MTS machine where the data is collected with a rate of 100 data points per second. The load and displacement data which collected from the test machine is fed to the non-destructive testing systems by using analog inputs.

Figure 3.1- Hybrid Non-Destructive Testing Setup

ii.   Acoustic Emission

Acoustic emission device used in this study is Micro-II digital AE System (Physical Acoustics Corporation). The AE data acquisition system consists of 4 channels AEWin DiSP system with two piezoelectric sensors, prea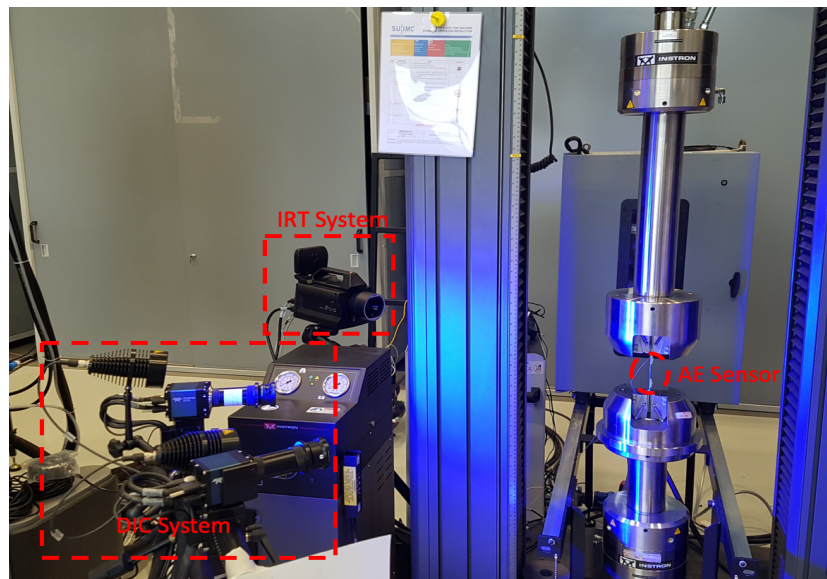mplifiers with 40db gain and 16 bit high speed A/D converters. Two piezoelectric sensors with a band range of 200-750 kHz and with a peak frequency of 500 kHz. These sensors are placed at the horizontal and vertical midpoints of the specimen and they were 45 mm apart from each other. Furthermore, the sensors are attached to the surface of the specimen by hot melt glue; these attachments should be done carefully because they directly affect the signal quality. The signals received are amplified automatically by using 2/4/6 AST preamplifiers which increases the power of the signal and eases the post processing. Also a threshold of 42db is set to minimize the undesired emissions such as mechanical vibrations. The calibration of the system is done to calculate the wave speed inside the specimen. This calibration is performed in accordance with ASTM E976, a specific point between the sensors is selected and the distances to the each sensor is measured and entered into the system. Then a 0.3 mm lead pencil is broken on the selected point, by using the AE data from the breakage and the distance to the source the system calibrates itself. Figure 3.2 shows AE testing controller, sensor and amplifier used in this study.

Figure 3.2- AE testing controller, sensor and amplifier

iii.   DIC

The DIC system was supplied from GOM: Optical Measuring Techniques. This device has two 12 megapixel monochrome cameras. Figure 3.3 shows the DIC test set-up used in this study. A tripod is used to stabilize the cameras during data acquisition. Before the experiment, the system is calibrated followed by the setting system parameters correctly. These parameters are working distance, camera separation distance, and camera angle. The first step of the calibration process is

syncing images from each camera. To do this, a laser is projected to a calibration block and the cameras are moved so that the beam is at the center point of each camera. Then the focuses of the cameras are set by adjusting the calibration block so that small size letters from a business card can be read clearly. The next step is the adjustment of lighting by opening the iris for camera for the appropriate exposure and aperture until the desired brightness is obtained. In the final step of calibration, the calibration block is tilted in horizontal and vertical axes in 13 different combinations by which the system calibrates itself for the movement in 3D space.
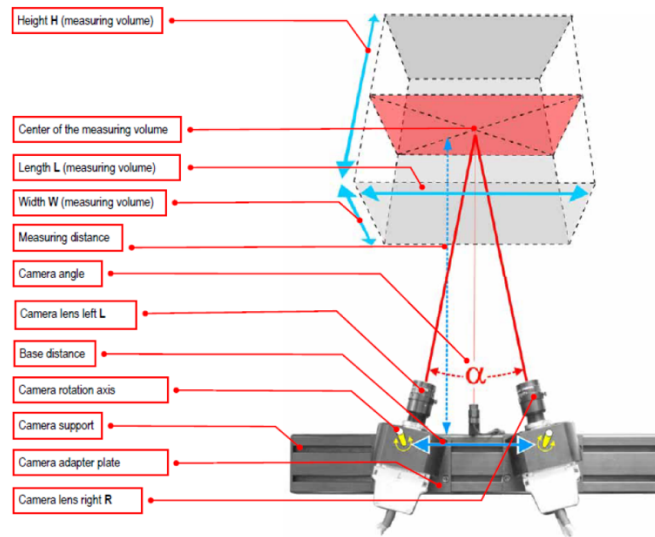
Figure 3.3- DIC test set-up

iv.   Infrared Thermography

Infrared thermography camera used in this study is x6580sc lnSb cooled 640x512 thermal camera manufactured by FLIR. The data acquisition was done at 100 Hz and 25 mK sensitivity.

3.2   Sample Preparation

Carbon fiber/epoxy laminates were produced with two different fiber orientations. The fiber orientations were shown in Figure 3.4 where CP denotes cross ply and QI denotes quasi isotropic sample. Specific fiber orientations were selected to highlight the effect of 0o and 45o plies. Due to previous experiences of edge cracking, outermost layer was selected to be in 0o orientation for both samples. This was especially important for these tests due to all non-destructive testing techniques using the outermost surfaces to collect data.

Sample	Layup
CP	$[0°/90°]_{2s}$
QI	$[0°/90°/45°/-45°]_{s}$

- - - - - Indicates Midplane of sample

Indicates Ply which damage begins

CP Sample	QI Sample
0°	0°
90°	90°
0°	45°
90°	-45°
90°	-45°
0°	45°
90°	90°
0°	0°

Figure 3.4- Stacking Sequence of each Sample

Sample were produced by hot press method. To this aim, prepregs were placed between two cleaned metal surfaces and a pressure of 3.5 tons was applied at 120C for 30 minutes. Then, the prepregs were left to cure under ambient temperature for 4 hours until the temperature cools down to 30C. Figure 3.5 shows the stacked carbon fiber/epoxy prepregs before the application of heat and pressure.
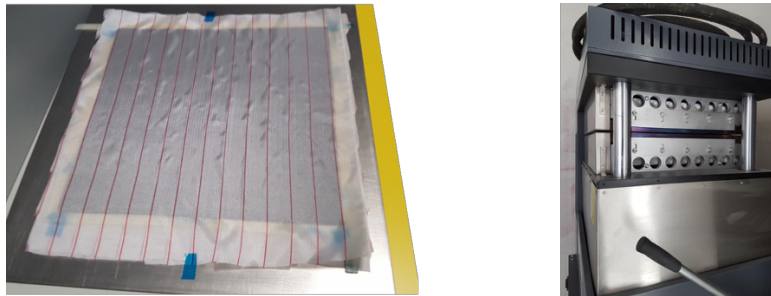
Figure 3.5- Stacked Plies ready for Hot Press [left] and Hot Press equipment [right]

The composite laminates were then cut into the tensile test specimens in accordance with ASTM D3039 standard. End tabs were adhesively bonded to the composite specimens to maintain more uniform stress distribution and to obtain final failure closer to the middle section of the specimens. Tensile tests were carried out on the prepared composite specimens with a crosshead speed of 1 mm/min.

CHAPTER 4

4   Results and Discussions

4.1   AE Results

Damage generates acoustic emission due to sudden changes in the material. Generated emissions propagate through the material in the form of elastic waves which are collected from the sample with piezoelectric sensors. These sensors are able to convert mechanical movement of the elastic waves in to electrical signal. Therefore, each elastic wave is stored as a waveform (Figure 2.3) which can be processed via signal processing tools.

The most basic signal processing features are amplitude and frequency. Amplitude is the magnitude of a waveform and the frequency is the oscillations per 1 second. For analyses purposes, the peak amplitude and peak frequency of the waveform is used. Peak amplitude is the maximum amplitude reached and peak frequency is the frequency at peak amplitude. Moreover, the amplitude of a waveform is collected as a voltage and then converted into decibel in order to better visualize the data. The amplitude deviations between different waveforms can be vary within 100 times of each other. Therefore, the voltage is scaled logarithmically to decibel (Equation 3) where waveform voltage is V_2 and a reference voltage is V_1.

$$dB = 20 \cdot log \frac{V_2}{V_1}$$

(3)

Figure 4.1 is the amplitude vs frequency graph for both CP and QI samples. Each data point at the graph is a waveform originated from acoustic emissions. The peak amplitude and frequency of the waveform is used to reflect the properties of the most dominant acoustic emission.
At first glance, waveforms of both samples look very similar even though they have different stacking sequences. The similarity can be an indication that the failure mechanisms of these samples are stacking sequence independent and more material dependent. The difference between these samples is marked with green and blue boxes. Green box indicates a frequency level that does not exist in CP sample but exists in QI sample. Therefore, it can be associated with the 45°

plies which do not exist in CP but exist in QI sample. Additionally, blue box is a frequency level that exists in CP sample but not in QI sample. Unfortunately, amplitude and frequency data is not enough to describe source of this deviation.
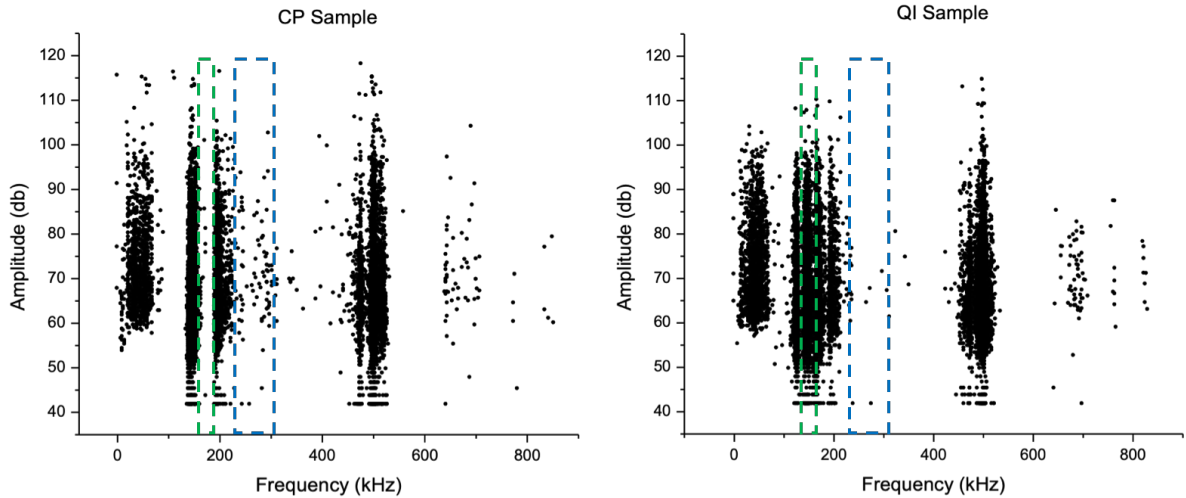

Figure 4.1- Amplitude vs Frequency Graph for CP and QI samples

In order to better characterize failure modes, it is also important to observe frequency features in time domain. Time domain will provide information on the state of the sample. As time proceeds, damage occurs on the sample and the AE activation time at frequency level can provide information on characterizing them. Figure 4.2 shows frequency vs time graph for CP and QI specimens. For both samples, from the beginning of the test, a wide variation of frequencies are active (marked with orange box in Figure 4.2). Most likely source of these waveforms is be the 90° ply in both samples because it is the weakest structural element in both samples and as it fails, a wide variation of frequencies (signifying matrix, interface and fiber failures) are be active. However AE related with 90° ply should not have high energy. Therefore, this point will be investigated at next section by checking AE energy. Differences in that were found between samples in Figure 4.1, are also present in Figure 4.2. These frequency regions are marked with green and blue boxes in Figure 4.2, as it was in Figure 4.1. Waveforms in the green box at QI sample were associated with 45° degree ply damage. Their activity starts around 40 second mark and continues until the end of the test in Figure 4.2. This finding supports the association between green box and 45 degree ply failure. Additionally, there is a new similarity between the samples that was observed at Figure 4.2. This region is marked with a purple box for both samples and it

indicates damage with high frequency, that occurs in a burst. The origin for these AE is not clear however, it will be further be investigated in later stages of the discussion.
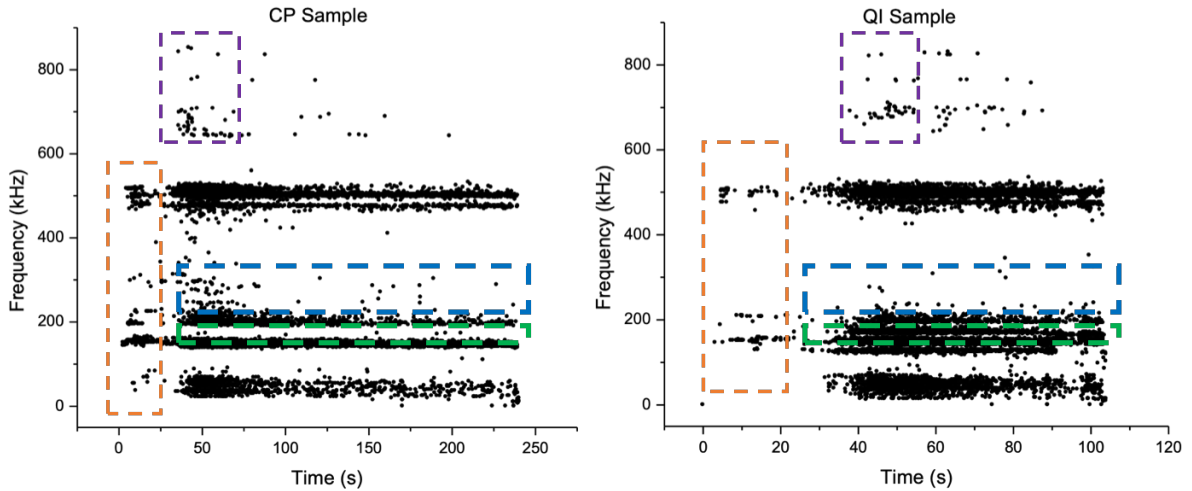

Figure 4.2- Frequency vs Time Graph for both CP and QI Samples

In order to acquire more accurate magnitude from the waveform, a different feature is introduced. Characterizing the amplitude of a waveform only displays the maximum magnitude reached within the waveform. This approach can lose data if the waveform is complex and have multiple frequencies (Figure 2.4). Therefore, signal energy of the waveform can be calculated by using the equation at Figure 4.3 (left). The feature is also visualized at Figure 4.3 (right) where the complete waveform is integrated to calculate the energy in terms of joules.

$$E = \int_{-\infty}^{\infty} |x(t)|^2 \, dt$$

Figure 4.3- Equation for signal energy (left), visual explanation of signal energy (right)[19]

Energy of a waveform is a more complete way to quantify damage. This is due to the relationship between energy and the load exerted on the source of an acoustic emission. There is a direct correlation between the amount of load that the source of an acoustic emission carries and the energy released by it. On the other hand, frequency is a great tool to characterize damage. Frequency of a waveform directly relates to the formation speed of an acoustic emission. Therefore, failure mechanisms that are inherently faster have higher frequencies such as fiber

17

failures and failure mechanisms that are inherently slow have lower frequencies such as matrix failures (Figure 2.5). [10-14]

In order to identify the dominant frequencies related with damage, a frequency ranged energy distribution graph is made (Figure 4.4). These energy values are calculated by summing up the energy of the waveforms at each frequency interval. As a result, Figure 4.4 shows the total energy at each frequency range for CP and QI samples. Each bar belongs to a frequency range and denotes magnitude of the energy.
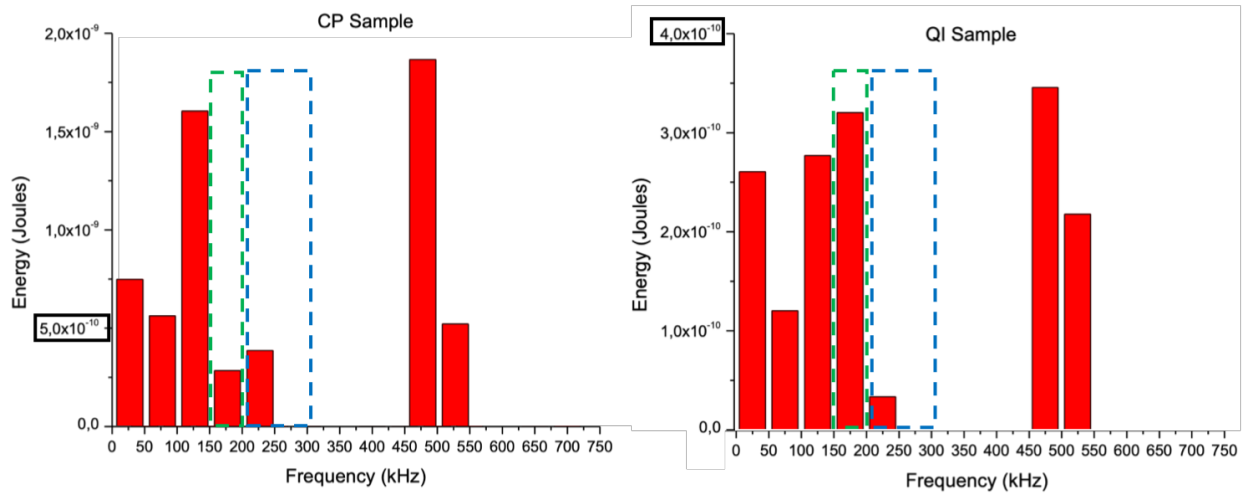

Figure 4.4- Frequency Histogram of Energy for both CP and QI Samples

At both samples 150-200 kHz and 450-550 kHz frequency range are high in energy. This range was associated with delamination related failures (150-200 kHz) and fiber related failures (450-550 kHz) at Figure 2.5 according to the work of Gutkin et al [11]. QI sample includes an additional energy peak at 150-200 kHz range (marked with green box in Figure 4.4). At Figure 4.1 this range was associated with damage due to the introduction of 45º ply. However fiber failures at 45º ply will manifest at 450-550 kHz frequency range. Therefore 150-200 kHz AE can be associated with additional delamination introduced due to the existence of 45º ply. Lastly, even though Figure 4.1 demonstrated the significance the 200-300 kHz frequency range (marked with blue box), energy magnitude is insignificant in terms of energy. Therefore effect of debonding related failures can be negated for these samples.
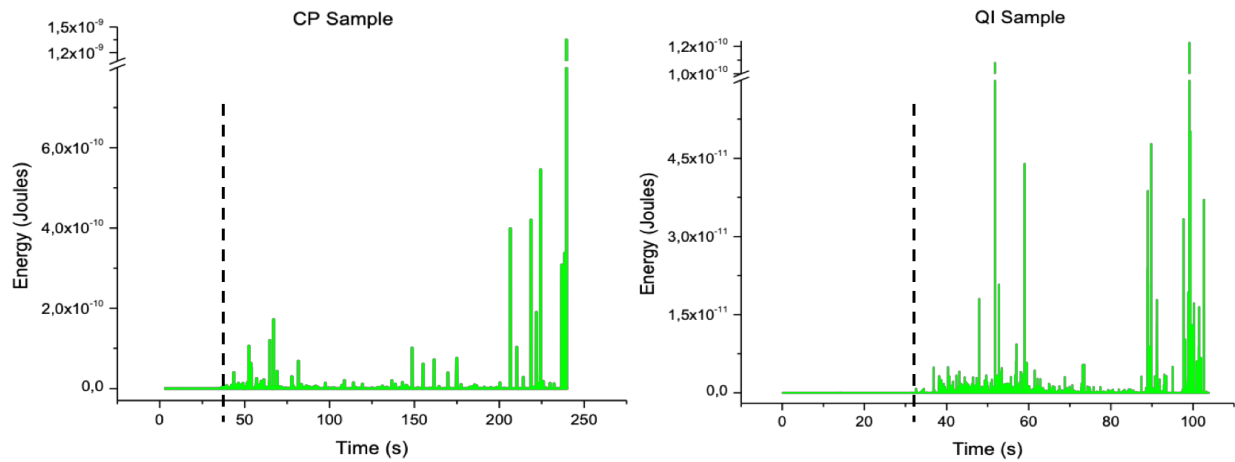
Figure 4.5- Stepwise cumulative Energy vs Time Graph for both CP and QI Samples

Frequency is a promising tool when characterizing the type of the failure mechanism. However, it cannot provide information regarding the magnitude of a damage. Therefore, the energy corresponding to these waveforms should be investigated. Figure 4.5 shows the stepwise cumulative energy vs time graph for both CP and QI samples. For each timestep, energy of all waveforms were cumulated then plotted in time domain. Therefore, progression of damage in terms of acoustic emission energy can be seen in time domain.

Figure 4.2 demonstrated that there are waveforms at the beginning of the test that relate with matrix, interface and fiber damages (marked with orange box). Figure 4.5 is demonstrating that these waveforms have no significant energy. This finding confirms the theory that these waveforms belong to a non-load bearing ply which for these samples is the 90 degree ply.

Figure 4.5 also demonstrates the point where damage starts on load bearing mechanisms. This point is marked with a black line in Figure 4.5. CP sample reaches this point at 40 second mark, QI sample reaches this point at 30 second mark. In terms of acoustic emission, these points act as marker that identifies onset of damage that effects structural integrity.
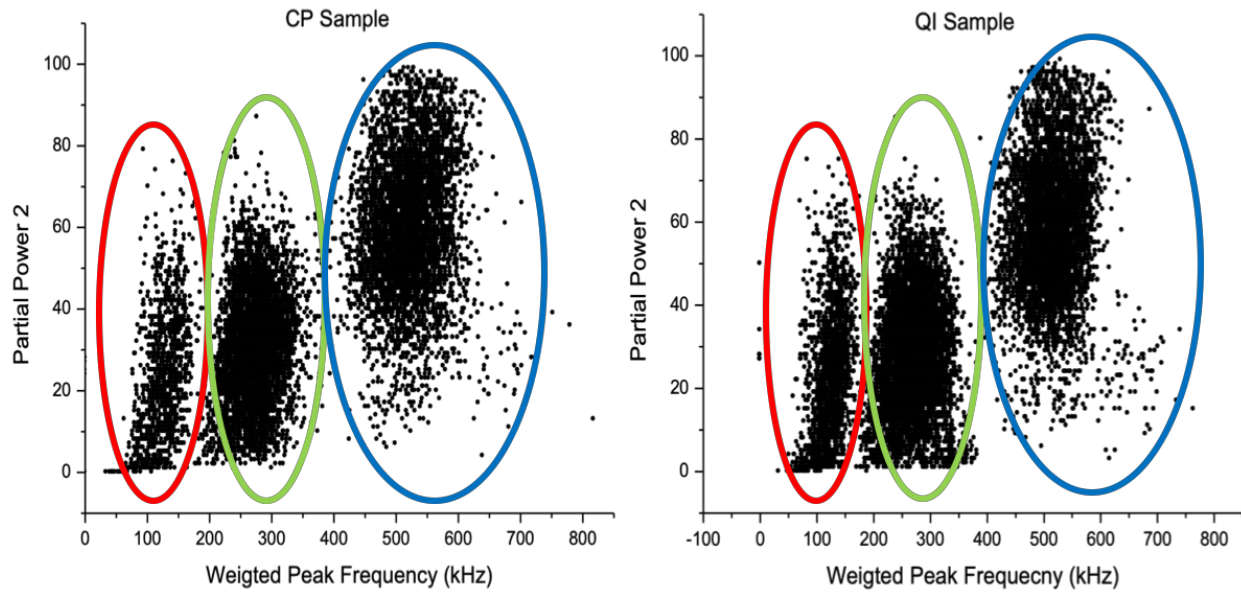
Figure 4.6- Partial Power 2 vs Weighted Peak Frequency Graph for both CP and QI Samples

Lastly, K-means clustering was performed on the AE data. Weighted peak frequency and PP2 are selected in accordance with the literature [11]. The outcome of the clustering was similar to the separation that could be observed from Figure 4.6 which shows PP2 vs f_{WFP} graph for both CP and QI Samples. Three clusters were formed which centered at low, mid and high end of the frequency spectrum. Cluster 1, Cluster 2 and Cluster 3 are respectively associated with matrix failures, interface failures (such as debonding and delamination) and fiber failures (such as fiber fracture or fiber pullout) (Figure 4.7).
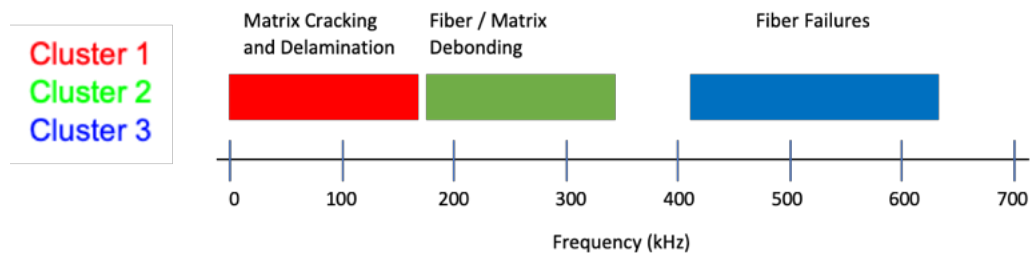

Figure 4.7- Identification of each Cluster

Clustering enables the visualization of the complete picture by providing another dimension to the data. Figure 4.2 and Figure 4.5 are able to demonstrate each data point only as frequency or energy. However, Figure 4.8 is able to combine these plots to provide a clearer

picture. For both samples, at the beginning of the test, there are multiple clusters of acoustic emissions (marked with black box at Figure 4.8) but the energy associated with these acoustic emissions are very low. Therefore, low energy damages of three clusters indicate damage at a non-load bearing ply which would be the 90° ply for both samples.
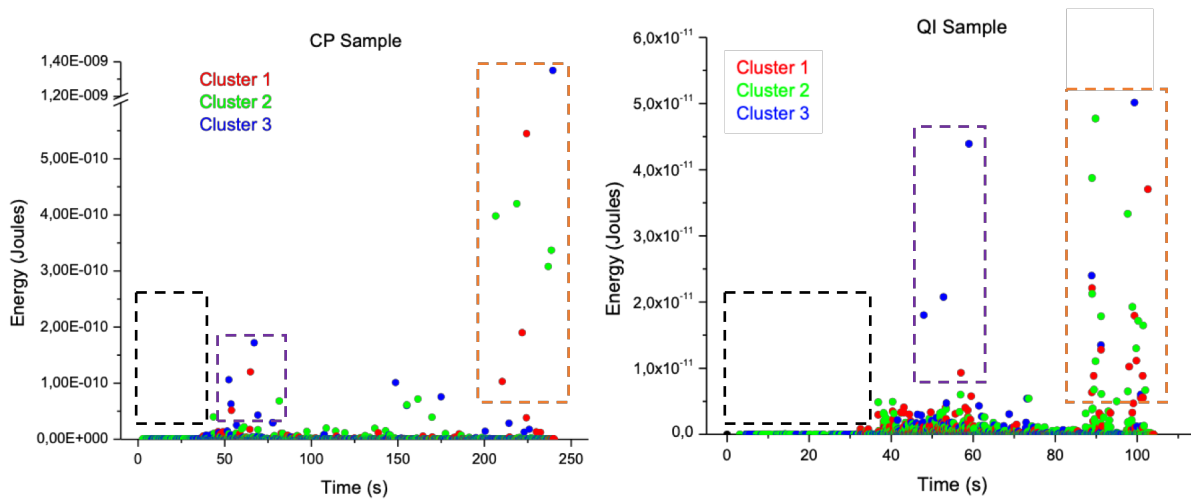

Figure 4.8- Clustered Energy vs Time for both CP and QI Samples

Lastly, for both samples at the end of the test, there are again multiple clusters of acoustic emissions (marked with orange box at Figure 4.8) with higher energy. These acoustic emissions indicate the dominant failure mechanisms that lead to fracture. Both samples have matrix/delamination (cluster 1) and fiber (cluster 3) based damages however, amount of fiber matrix debonding (cluster 2) related damages is significantly high for QI sample at fracture.

4.2 DIC Results

DIC was used to gather the traditional strain data in non-contact means. Full field strain for both samples at each time step (as shown in Figure 2.7) were calculated by using the DIC system. Then, in order to quantify the stain value for each time step, full field strain was averaged. Strain data for both samples are linear and without deviation. In order to identify critical points in terms of strain, stepwise change in strain was calculated by taking the first derivative of strain with respect to time. Therefore, change in strain for each time step was calculated.

Stepwise change in strain for each time step is shown in Figure 4.9. For both samples, the point of load exertion is indicated by a sharp peak at the beginning (marked with green box in

Figure 4.9). Then there is a trend of, gradually decreasing strain until fracture. At fracture there is a sharp increase in strain for QI sample but there is no change in CP sample (marked with orange box in Figure 4.9). Stability of the CP sample at the end of the test could be due to test being stopped before the complete fracture of the sample. The most obvious deviation in stepwise change in strain is marked with a blue box in Figure 4.9. At this point there is a significant drop in stepwise strain rate however, the root cause of this change is unknown.
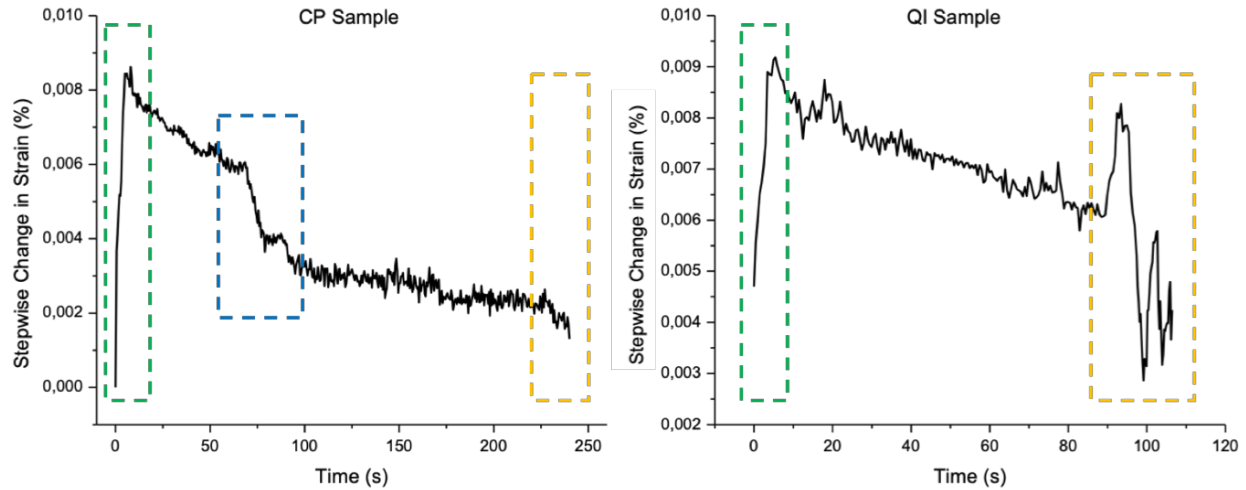
Figure 4.9- Stepwise Change in Strain Graph for both CP and QI Samples

Furthermore, full field average strain data then used to calculate the stiffness for each sample. Figure 4.10 shows stress vs strain graphs for both CP and QI Samples. Stiffness of CP sample is 64 GPa and ultimate tensile stress is 1220 MPa. Stiffness of the QI sample is 51 GPa and the ultimate tensile stress is 710 MPa. As it is expected, stiffness of the CP sample is much higher than the QI sample.

.

Figure 4.10- Stress vs Stain Graphs for both CP and QI Samples

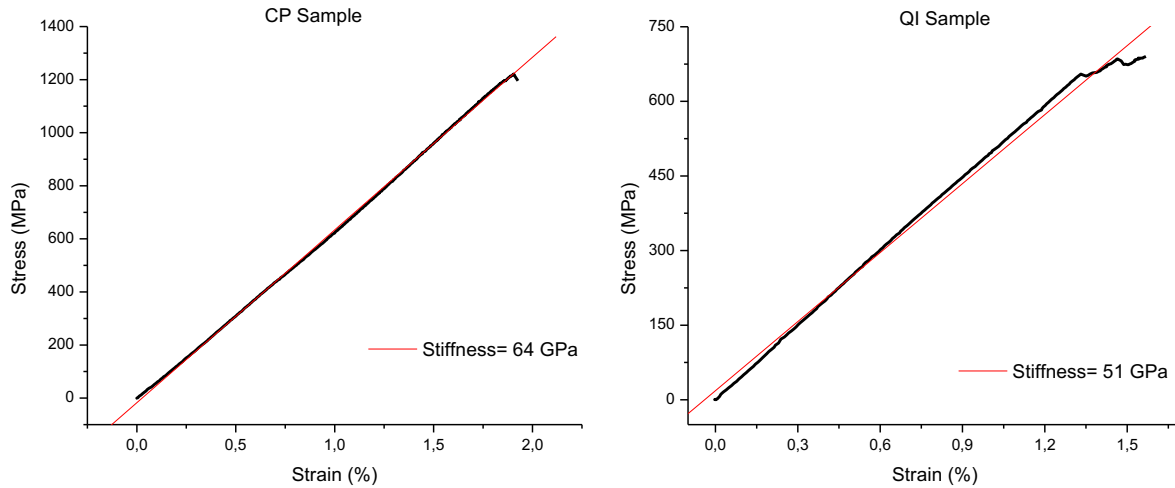Stiffness is a linear data with small deviations that could be used as a marker for damage. Therefore small deviations at stiffness could be amplified by calculating stiffness rate by taking its first derivative with respect to strain. A decrease in stiffness rate correlates with an instantiations energy release. At the onset of damage, stress remains the same however, the load bearing unit relaxes by a sudden increase of strain. Decrease in stiffness correlates with the redistribution of stress within the material where stress gets under control and increase in strain slows down. Next iteration of this relationship is crack propagation. At crack growth, crack opens with a sudden decrease in stiffness, then stress gets redistributed within the structure which results an increase in stiffness.

Figure 4.11 is clearly able to define the initiation of fracture. These regions are marked with an orange box for each sample. For QI sample the deviation at fracture is so high that it can be seen in Figure 4.10. However, the deviation at fracture for CP sample is not visible in Figure 4.10 and it can only be seen after the introduction of stiffness rate feature.
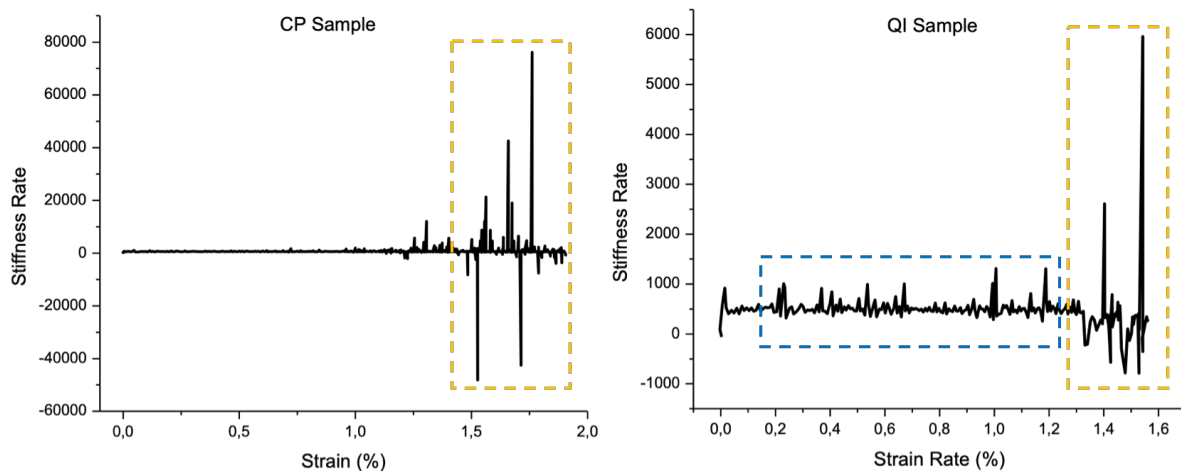
23

Figure 4.11- Stiffness Rate Graph for both CP and QI Samples

These results are exemplary for showing the benefit of DIC which is to gather data from the complete surface of the sample to detect the onset of damage. Other strain measurement techniques can only focus on a certain section of a material. Therefore, the value of DIC as a surface based damage marker is clear. However, DIC is not a volumetric measurement technique therefore, it is only able to quantify the surface damage.

4.3   IRT Results

There is an indirect relationship between temperature and stress. However, after damage starts to occur within a material, temperature then starts to increase. To highlight the change in temperature, delta temperature was calculated. This was done by first calculating the full field average temperature of each sample from the thermal camera system. Then subtracting each temperature iteration from the initial temperature. Delta temperature for both samples is shown in Figure 4.12 where the general trend for both samples is similar. Temperature first decreases down to damage stress point, then it stabilizes and finally it increases.

The point where decrease in temperature loses its linearity is the damage stress point. Damage stress point for the CP is at 40 seconds, 0.4% strain and -0.35 Celsius. For the QI sample it is at, 30 seconds, 0.52% strain and -0.2 Celsius. CP sample has a higher delta temperature at damage stress point. This is due the stiffness of the CP sample or in other words, its ability to undertake more stress before the damage stress point.
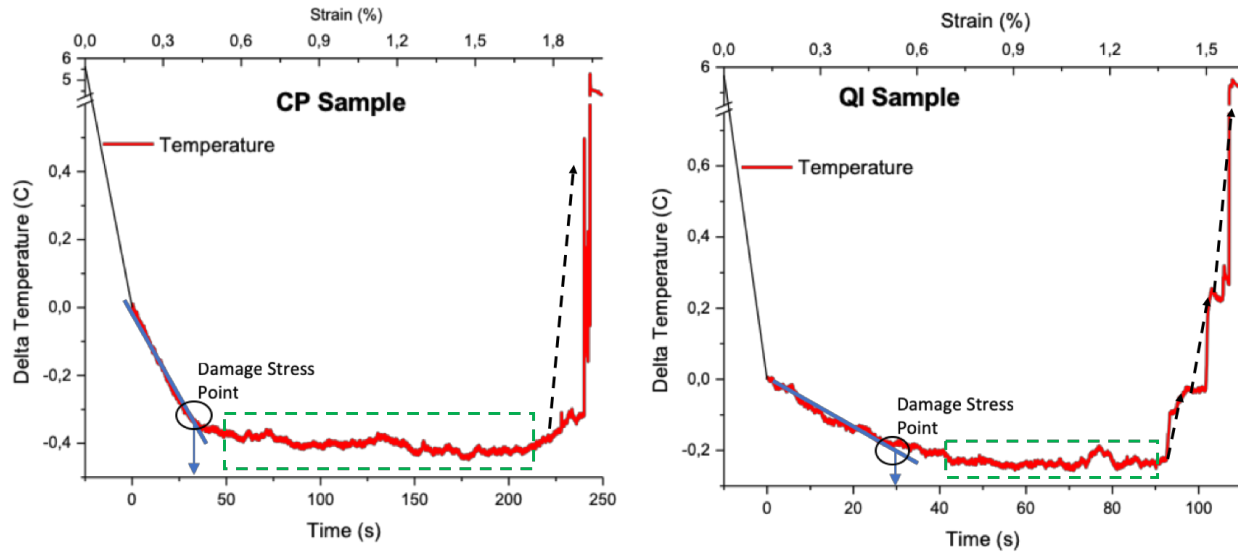
Figure 4.12- Delta Temperature Graph for both CP and QI Samples

After damage stress point, there are small deviations in temperature. However, temperature continues to be linear until the beginning of fracture. Fracture of both samples can clearly be seen due to the peak in temperature at the end of the test. However, speed of temperature increase to the maximum temperature differentiates these samples. For CP sample temperature instantaneously increases (marked with black arrow). On the other hand, for QI sample temperature increases in 3 steps (marked with black arrow). Reason behind this difference will be explored in the next section by using data from other techniques.

4.4 Coupled Results

AE and IRT are both volumetric techniques. They gather the most complete picture from within the sample. IRT has a damage marker (damage stress point) that indicates the initiation of damage within the sample. Moreover, AE has a damage marker which is the onset of high energy damage. These two markers are aligning in Figure 4.13 where damage stress point is marked with a dashed line in for both samples. Additionally, the relationship between these two methods is also clear at the fracture of the QI sample. As temperature increases in steps, acoustic emission energy is also peaking in steps. The relationship between acoustic emission and temporal change hasn't been explored in the literature. Therefore, it is a novel approach to verify the onset of damage with

these techniques. In the literature damage stress point was previously studied [15] which for CP sample is 370 MPa and QI sample 250 MPa.
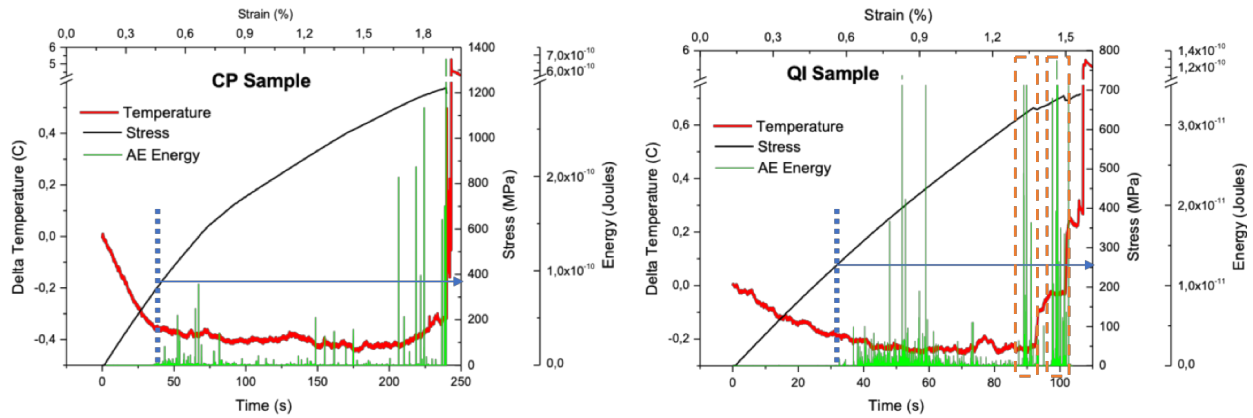

Figure 4.13- Energy vs Temp vs Stress Graphs for both CP and QI Samples

Following figures will be focusing on the complementary nature of these techniques. Thermography is a quantitative method that is very sensitive towards changes in energy and acoustic emission is a qualitative method that specializes on determination of damage sources. Figure 4.14 focuses on this relationship between these techniques. In terms of the overall test, after the damage stress point, emissions with higher order of energy are appearing and simultaneously the drop in temperature is decreasing. The clear relationship between acoustic emission and temporal energy can be observed at 50 second and 160 second marks.

Moreover, Figure 4.14 also contains stiffness rate data that provides information regarding the integrity of the surface of the sample. High deviations of the stiffness rate indicates damage activity on the surface which is a sign of decreasing structural integrity. Stiffness rate data is an important marker at CP sample due to the abundance of uniaxial fibers. Fiber breakage manifests as a sudden increase in stiffness rate, temperature and acoustic emission activity as shown in Figure 4.14
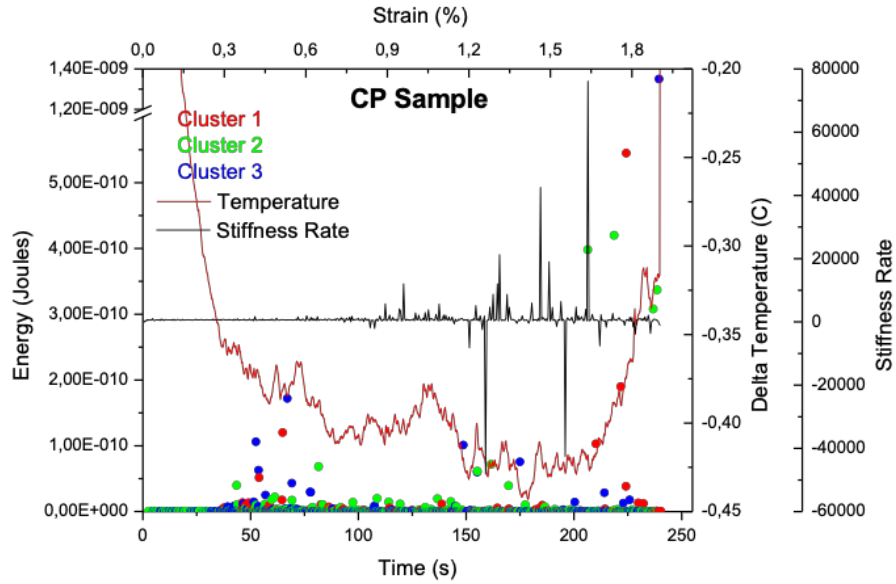
Figure 4.14- Temperature vs AE vs Stiffness rate for CP sample

At the end of the test there are simultaneous changes, in stiffness rate, temperature and acoustic emission activity. This relationship can better be observed by investigating the temperature data visually to quantify the damage mechanism. To this aim, points with significant temperature increase were marked (with blue line) at Figure 4.15 and thermal images of mentioned time stamps are in Figure 4.16. Each time stamp in Figure 4.15 shows a fiber failure thus explains the activity in stiffness rate.
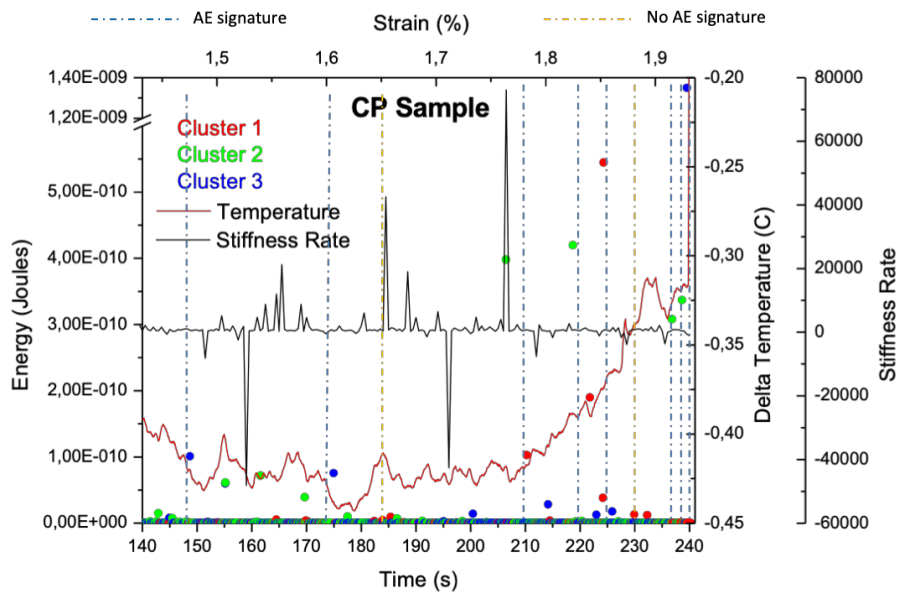

Figure 4.15- Temperature vs AE vs Stiffness rate for CP sample at Failure region

However, at time stamps that are marked orange in Figure 4.15 no emission signatures were recorded. This is most likely due to the inability of acoustic emission reaching the piezoelectric sensor. However, thermal data was able to demonstrate that these points had fiber failures. At all other points that have an emission, thermal data is able to provide the location of the damage and relative magnitude in terms of temperature.
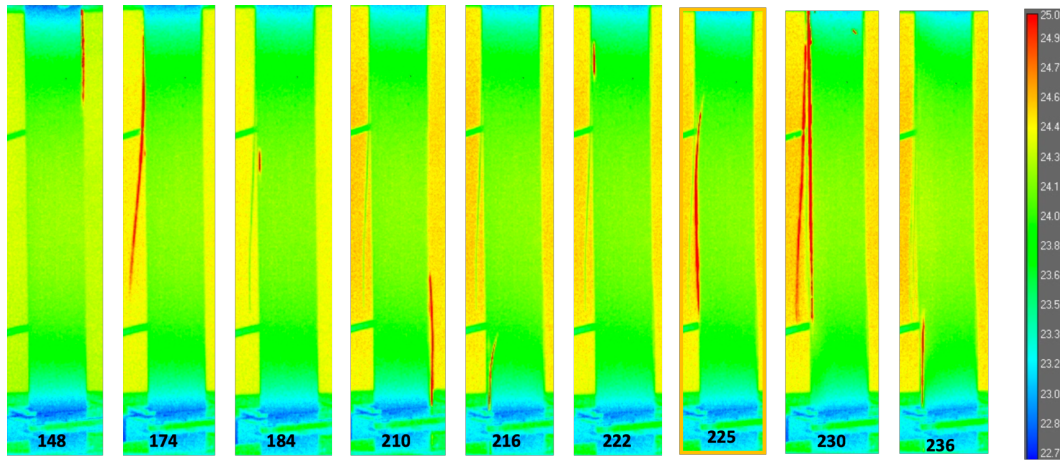

Figure 4.16- Thermal Images of CP sample at various time stamps

Consequently Figure 4.17 divides the lifetime of the CP sample into 3 sections based on the observations made regarding the damage progression. The first stage is the initiation where the material behaves quasi elastic and temperature drops due decrease in internal energy of the sample. At this stage damage occurs on the sample however, damage at initiation stage has low energy and has no effect on the structural integrity (demonstrated by AE data in Figure 4.13). Initiation stage ends with the damage stress point where the high energy damage start to occur. At progression stage, thermal energy of damages increase high enough to stop the decrease in temperature due to the work done by the sample on the surrounding and similarly the energy of the acoustic emissions also increase. The stage of fracture starts with the onset of deviations at stiffness rate. Structural integrity of the sample has deteriorated significantly and consequently there is visible damage on the surface.
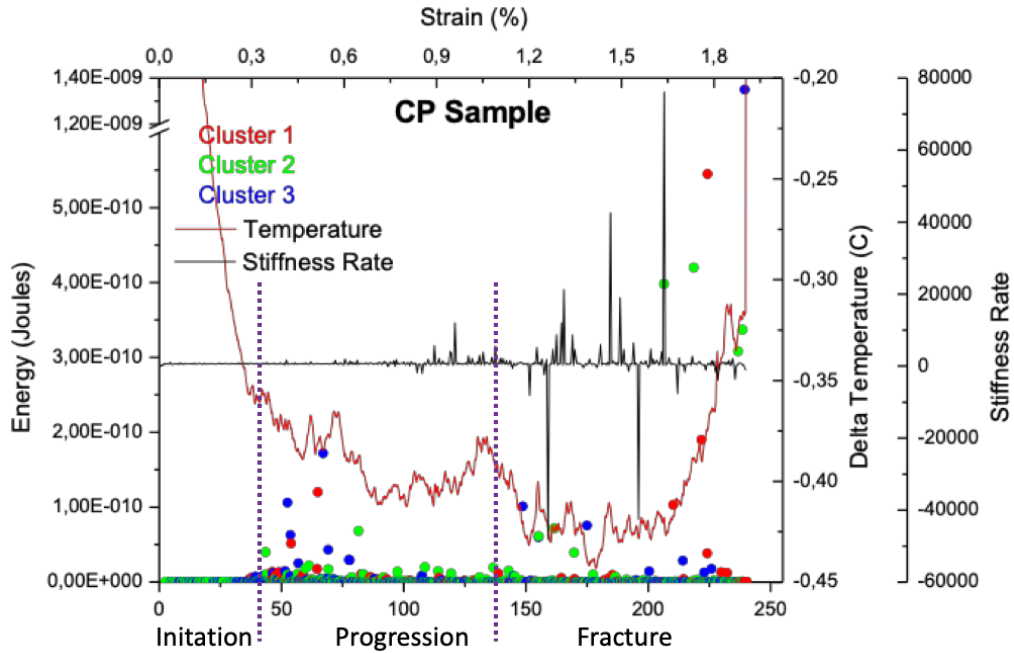
Figure 4.17- Stages of Lifetime for CP sample

Similar study of damage progression was also done for the QI sample. Figure 4.18 exhibits the decrease in temperature, increase in emission energy then lastly the onset of deviation of stiffness rate. Even though the general progression is similar for both samples, the mechanism of fracture has to be different. QI sample is less stiff and more prone to inter layer failures due to existence of a third orientation type. Therefore, the fracture of QI is also analyzed in detail by using thermal images.

Figure 4.18- Temperature vs AE vs Stiffness rate for QI sample

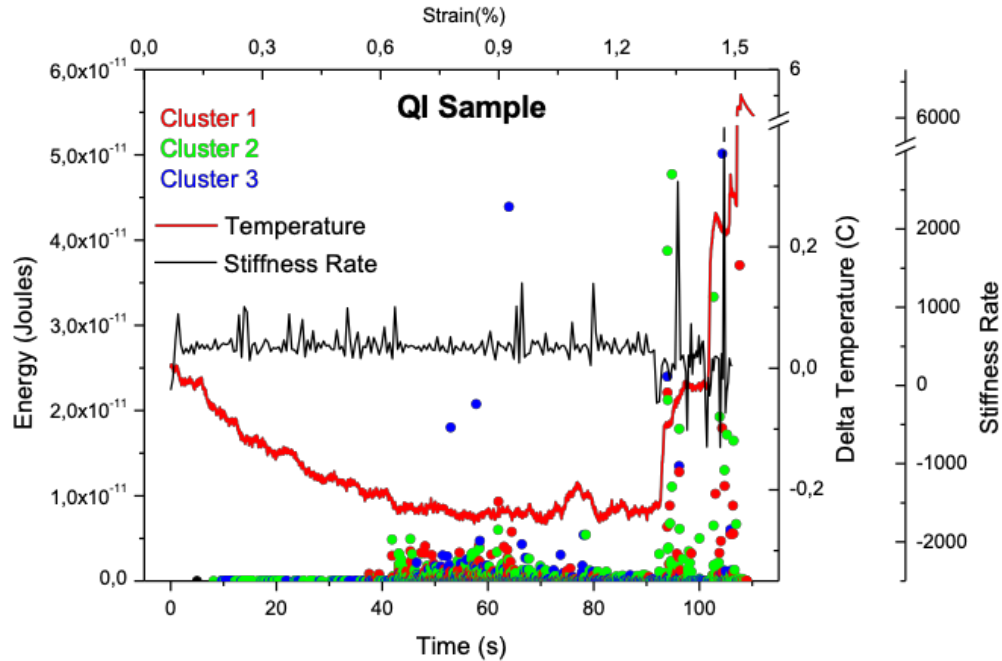Time stamps with significant temperature increase were given in Figure 4.19. Figure 4.20 shows the thermal images at these time stamps. Debonding of a layer can be seen at between time stamp 93 – 96 and 102 – 104. These ranges are marked with a blue circle in Figure 4.19. At these ranges, there is a clear emission signature of debonding denoted by cluster 2. However, the magnitude of the damage could only be quantified after noticing the increase in temperature and the extent of the damage could only be quantified by investigating thermal images.

Moreover, time stamp 105 shows the fracture of the sample by a fiber failure where the change in temperature is concentrated at a single region. This image is also supported by a high energy emission that is cluster 3 which relates with fiber failures. Therefore, the fracture of this sample can be considered to occur in two phases. First is interlayer debonding which is labeled by a green bar, then a fiber based failure which is labeled by a blue bar. This analyses explains how the fracture of QI sample is occurring in stages (shown with black arrows in Figure 4.12).

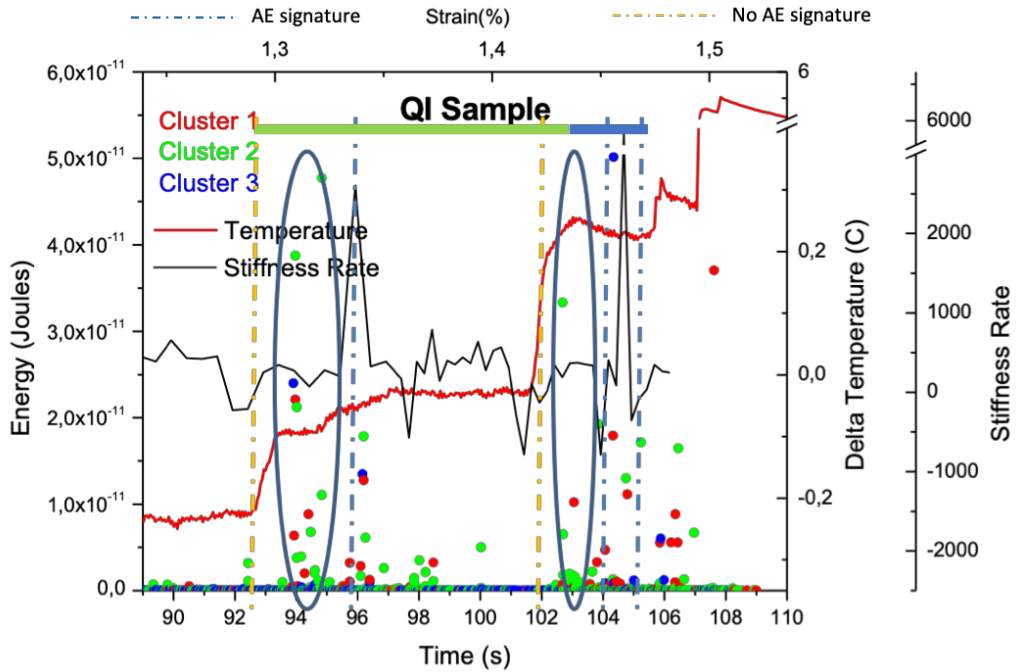*Figure 4.19- Temperature vs AE vs Stiffness rate for QI sample at Failure region*

Additionally similar to CP sample, there are couple time stamps with no emission signature (orange dashed line in Figure 4.19). These are most likely due to the elastic waves of AE, not being able to reach the piezoelectric sensor due to air gaps caused by extensive damage.
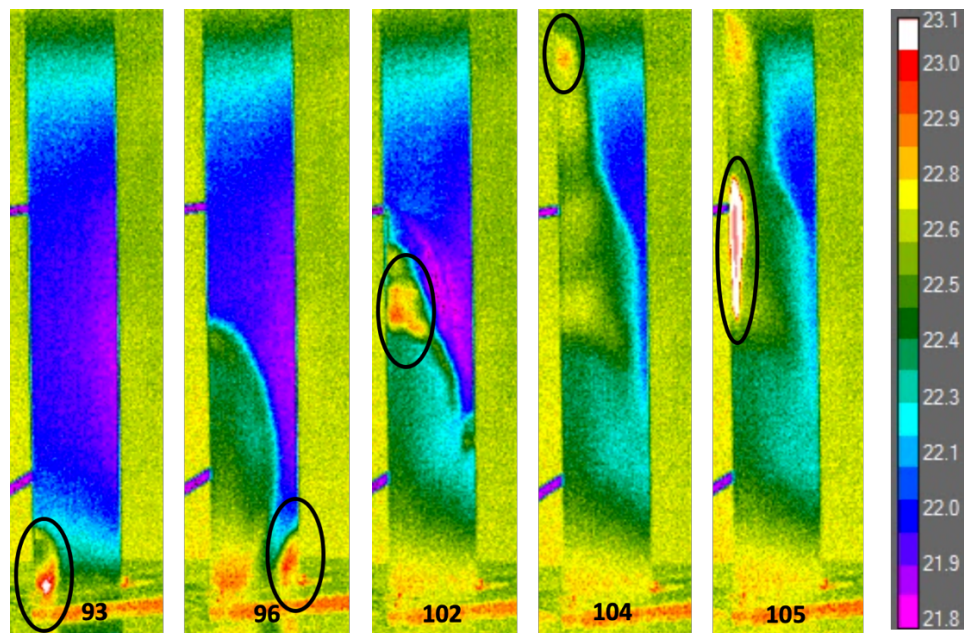
Figure 4.20- Thermal Images of QI sample at various time stamp

Similar to the CP sample, Figure 4.21 divides the lifetime of the QI sample into 3 sections. At initiation stage material behaves quasi elastic until the damage stress point. At progression stage, there is a high density of emissions together with decrease in temperature drop. The stage of fracture starts with the deterioration at the structural integrity of the sample which is indicated by deviations at stiffness rate. It should also be noted that at the third stage of the QI sample there is significant debonding activity (indicated by cluster 2) due to presence of 45° plies.

Figure 4.21- Stages of Lifetime for QI sample

CHAPTER 5

5   **Conclusion**

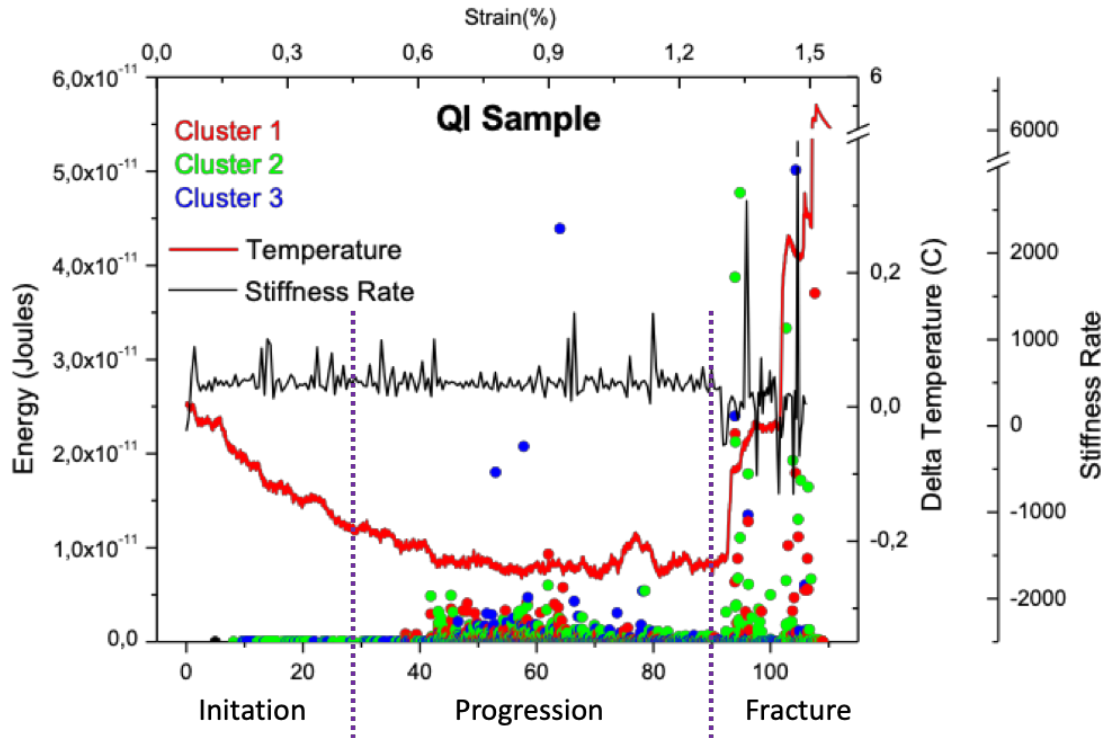This thesis focused on the relationship between three non-destructive testing techniques that can detect three different types of energy manifestation due to damage. It demonstrated that AE is able to characterize damage. This theses performed characterization by clustering and consequently defined 3 different origins of damage. This allowed pinpointing of each instance of fiber failure, interface failure or matrix failure. Additionally, AE detected activities of different and similar ranges of frequencies between CP and QI sample. Therefore, existence of a specific frequency region was shown due to 45º plies. Moreover, low energy and wide frequency range activity of 90º ply was demonstrated. Furthermore, AE was able to mark the onset structurally significant damage. In the literature, this ability was also associated with IRT. Therefore, the relationship between these methods are shown in terms of detecting the onset of structurally significant damage. Structurally insignificant damage is in other words is reversible. At this reversible rage, IRT was able to detect the system doing work on the sample in means of decrease in temperature. Onset of damage is detected by the change of the decrease in temperature rate. As damage occurs on the sample, the sample starts doing work on the system. Therefore, temperature of the sample starts increasing with each damage occurrence as decrease in temperature continues due to continuous nature of reversible (elastic) deformation. Additionally, IRT is also able to get full field temperature images for each time step. This feature was able to support AE for characterization. AE is effective into characterizing each damage. However, it cannot provide information if detected damage are related with each other in terms of a significant fracture. Clearest example was observed in QI sample where two significant debondings occurred. AE was able to detect and increased activity of debonding signature. However, IRT was able to detect debonding starting from left side of the sample and moving towards the right side until a complete ply is deboned. At this stage DIC also started to detect damage in terms of stiffness rate. As the surface of the sample deformed, stiffness rate decreases then increases that respectively corresponds with crack opening and closing.

In conclusion, within the scope of this thesis, 2 stacking sequences were tested under hybrid non-destructive testing techniques. Test results provided important markers that could detect damage. Coupled with literature, detected damages were able to be characterized to conclusively

identify tensile behavior of two stacking sequences. Two novel approaches were present. First was the use of stiffness rate to detect the onset of surface damage. Second was the detection of damage stress point with AE. This point is a feature of IRT and it indicates the onset of structurally significant damage. Therefore by using these two points, life of any sample can be split up to 3 regions. Damage first initiates with damage stress point, then it progresses and fracture begins with significant deviation at stiffness rate.

6   Future Work

There has been a couple novel approaches within this thesis. These are the usage of stiffness rate and the demonstration of the relationship between acoustic emission and thermography. Stiffness rate parameter should be explored with fracture tests that can take more advantage of this feature. A compact tension test can prove the relationship of the parameter to crack growth and fracture. On the other hand the relationship between acoustic emission and thermography has a lot of potential. Thermography is able to fill in the one big shortcoming of acoustic emission, which is the ability of quantifying damage. Additionally, it is also a volumetric technique. Thermography will be able to quantify and acoustic emission will be able to qualify damage.

There is also work to be done in terms of the effect of stacking sequence on the lifetime and failure mechanisms. The simplest forms of different orientations should be tested to observe the purest stacking based AE features. Unidirectional samples of both 0 and 90 degrees should be tested with the same experimental setup.

References

[1]   Boeing. Boeing 787: from the ground up; 2008. [12.07.13]

[2]   Department of defense. composite materials handbook: polymer matrix composites materials usage, design, and analysis. Vol. 3. N.p.: n.p., 2002. Print.

[3]   R. K. Miller, Nondestructive Testing Handbook, 2nd edition, Volume 5 "Acoustic Emission Testing." 1987. American Society for Nondestructive Testing, Columbus, OH.

[4]   Scala, C.M. and R.A. Coyle, Acoustic emission waveform analysis to identify fatigue crack propagation in a mirage aircraft: Journal of Acoustic Emission, Vol. 6, No. 4

[5]   2016 Practical Acoustic Emission Testing: Springer Japan

[6]   Vanniamparambil, P. (2014). A Novel Coss-Vlidated Nondestructive Evaluation Framework for Damage Detection using Acoustic Emission

[7]   Acoustic Emission Testing. Basics for Research-Applications in Civil Engineering, C. Grosse and M. Ohtsu. 2008: Springer Berlin Heidelberg.

[8]   Acoustic Emission Testing. Third ed. Nondestructive Testing Handbook, P. Moore. Vol. 6. 2005.

[9]   Hellier, C., Handbook of Nondestructive Evaluation, 2003, McGraw-Hill.

[10]   Roberts, T.M. and M. Talebzadeh, Acoustic emission monitoring of fatigue crack propagation. Journal of Constructional Steel Research, 2003. 59(6): p. 695-712.

[11]   Gutkin, R., Green, C., Vangrattanachai, S., Pinho, S., Robinson, P., & Curtis, P. (2011). On acoustic emission for failure investigation in CFRP: Pattern recognition and peak frequency analyses. Mechanical Systems And Signal Processing, 25(4), 1393-1407. doi: 10.1016/j.ymssp.2010.11.014

[12]   Kempf, M., O. Skrabala, and V. Altstadt, Acoustic emission analysis for characterization of damage mechanisms in fibre reinforced thermosetting polyurethane and epoxy. Composites Part B-Engineering

[13]   Sause, M.G.R., et al., Pattern recognition approach to identify natural clusters of acoustic emission signals. Pattern Recognition Letters, 2012. 33(1): p. 17-23.

[14]   Sause, M.G.R., et al., Quantification of failure mechanisms in mode-I loading of fiber reinforced plastics utilizing acoustic emission analysis. Composites Science and Technology, 2012. 72(2): p. 167-174.

[15] Risitano, A., Giacomo, R., & Clienti, C. (2010). Fatigue limit by thermal analysis of specimen surface in mono axial traction test. EPJ Web Of Conferences, 6, 38010. doi: 10.1051/epjconf/20100638010

[16] Loutas, T., et al., Damage evolution in center-holed glass/polyester composites under quasi-static loading using time/frequency analysis of acoustic emission monitored waveforms. Composites science and technology, 2006. 66(10): p. 1366-1375.

[17] Shoeb, A., & Clifford, G. (2006). Wavelets; Multiscale Activity in Physiological Signals. Biomedical Signal And Image Processing Spring 2005, (Spring 2005).

[18] Time Frequency Analysis. (2019). Retrieved from https://www.wavemetrics.com/products/igorpro/dataanalysis/ signalprocessing/timefrequency

[19] Langton, C. (2000). Signal Processing & Simulation Newsletter